

# Structural Characterization of Microemulsions in a Ternary System of Zn(oct-en)<sub>2</sub>Cl<sub>2</sub> Complex/Benzene/Water

Yoshiteru Ikeda,<sup>†</sup> Toyoko Imae,<sup>\*,†,‡</sup> JingChen Hao,<sup>†</sup> Masayasu Iida,<sup>§</sup>  
Tomomi Kitano,<sup>§</sup> and Naoko Hisamatsu<sup>§</sup>

Graduate School of Science and Research Center for Materials Science, Nagoya University,  
Nagoya 464-8602, Japan, and Department of Chemistry, Faculty of Science,  
Nara Women's University, Nara 630-8506, Japan

Received February 1, 2000. In Final Form: June 21, 2000

Microemulsions in a ternary system of bis(*N*-octylethylenediamine)zinc(II) chloride (Zn(oct-en)<sub>2</sub>Cl<sub>2</sub>)/benzene/water were investigated by transmission electron microscopy, atomic force microscopy, infrared absorption spectroscopy, and the Fourier transform pulsed-gradient spin-echo NMR method. W/O microemulsion, sponge, and bicontinuous structures were observed to have formed in the ternary system. At the interface of the benzene and water domains in the bicontinuous structure, hydrocarbon chains of *cisoid*Zn(oct-en)<sub>2</sub>Cl<sub>2</sub> were arranged, maintaining a 6 Å separation. The diffusion coefficient of water decreased in the following order depending on the water domain size: sponge; bicontinuous; W/O microemulsion structures.

## Introduction

Metal complexes are valuable as catalysts in biological and industrial reactions. Moreover, assembled systems of metal complexes are the focus of research interest due to their polymeric structures<sup>1–6</sup> and novel functionalities, such as liquid crystal formation<sup>7–10</sup> and molecular magnetism.<sup>11–14</sup> These assemblies, which are three-dimensional supramolecular complexes, are formed by noncovalent interactions, such as hydrogen bonds, stacking interactions, and metal–ligand coordination.

Introduction of hydrophobic hydrocarbon chains in hydrophilic metal complexes is a convenient method for constructing molecular assemblies. For this purpose, Langmuir monolayer and Langmuir–Blodgett (LB) films have been investigated for amphiphilic metal complexes including metallosoaps.<sup>15–20</sup> Deschenaux et al.<sup>15</sup> synthesized an amphiphilic cobalt complex and characterized

the structure of LB films using spectroscopy, microscopy, and small-angle X-ray scattering. A structural investigation of an amphiphilic metal complex has also been carried out by Werkman et al.<sup>17</sup> The molecular arrangements of amphiphilic copper and cadmium complexes were compared between LB films before and after polymerization. Soyer et al.<sup>19</sup> reportedly observed spin conversion in an LB film of an amphiphilic iron complex. Haga et al.<sup>20</sup> confirmed metal coordination from the subphase to the Langmuir monolayer of an amphiphilic ruthenium complex at the air–water interface. In addition, a series of double-chain amphiphilic octahedral cobalt complexes, bis(*N*-alkylethylenediamine)cobalt(III) salts, was prepared by Jaeger et al.,<sup>18</sup> who examined the *cisoid/transoid* diastereomer ratio according to the reaction solvent used. The surface pressure–molecular area isotherm of the *cisoid* species differs from that of the *transoid*. Xu et al.<sup>21</sup> observed bilayer membrane formation of *N*-alkylethylenediamine in both dilute aqueous Cu(NO<sub>3</sub>)<sub>2</sub> and acidic solutions, which suggested the presence of bilayer packing structures.

On the other hand, one (M.I.) of the authors of the present study<sup>22,23</sup> synthesized bis(*N*-octylethylenediamine)zinc(II) chloride (Zn(oct-en)<sub>2</sub>Cl<sub>2</sub>, (oct-en)<sub>2</sub> = CH<sub>3</sub>-(CH<sub>2</sub>)<sub>7</sub>NH(CH<sub>2</sub>)<sub>2</sub>NH<sub>2</sub>), which is insoluble in water but somewhat soluble in benzene and highly soluble in chloroform.<sup>22</sup> However, its solubility in organic solvents increases with the addition of an appropriate quantity of

\* To whom correspondence should be addressed. E-mail: imae@chem2.chem.nagoya-u.ac.jp. Tel: 81-52-789-5911. Fax: 81-52-789-5912.

<sup>†</sup> Graduate School of Science, Nagoya University.

<sup>‡</sup> Research Center for Materials Science, Nagoya University.

<sup>§</sup> Nara Women's University.

(1) Zarges, W.; Hall, J.; Lehn, J.-M.; Bolm, C. *Helv. Chim. Acta* **1991**, *74*, 1843.

(2) Baxter, P.; Lehn, J.-M.; DeCian, A.; Fischer, J. *Angew. Chem., Int. Ed. Engl.* **1993**, *32*, 69.

(3) Kramer, R.; Lehn, J.-M.; DeCian, A.; Fischer, J. *Angew. Chem., Int. Ed. Engl.* **1993**, *32*, 703.

(4) Bell, T. W.; Jousselein, H. *Nature* **1994**, *367*, 441.

(5) Lehn, J.-M., Atwood, J. L., Davies, J. E. D., Eds. *Comprehensive Supramolecular Chemistry*; Pergamon: London, 1995.

(6) Barbour, L. J.; Orr, G. W.; Atwood, J. L. *Nature* **1998**, *393*, 671.

(7) Koine, N.; Iida, M.; Sakai, T.; Sakagami, N.; Kaizaki, S. *J. Chem. Soc., Chem. Commun.* **1992**, *23*, 1714.

(8) Iida, M.; Sakai, T.; Koine, N.; Kaizaki, S. *J. Chem. Soc., Faraday Trans.* **1993**, *89*, 1773.

(9) Atencio, R.; Barbera, J.; Cativiela, C.; Lahoz, F. J.; Serrano, J. L.; Zurbano, M. M. *J. Am. Chem. Soc.* **1994**, *116*, 11558.

(10) Imae, T.; Ikeda, Y.; Iida, M.; Koine, N.; Kaizaki, S. *Langmuir* **1998**, *14*, 5631.

(11) Ohba, M.; Maruono, N.; Okawa, H.; Enoki, T.; Latour, J.-M. *J. Am. Chem. Soc.* **1994**, *116*, 11566.

(12) Ohba, M.; Okawa, H.; Ito, T.; Ohto, A. *J. Chem. Soc., Chem. Commun.* **1995**, 1545.

(13) Verdaguier, M. *Science* **1996**, *272*, 698.

(14) Sato, O.; Lyoda, T.; Fujishima, A.; Hashimoto, K. *Science* **1996**, *272*, 704.

(15) Deschenaux, R.; Masoni, C.; Stoeckli-Evans, H.; Vaucher, S.; Ketterer, J.; Steiger, R.; Weisenhorn, A. L. *J. Chem. Soc., Dalton Trans.* **1994**, 1051.

(16) Mori, O.; Imae, T. *Langmuir* **1995**, *11*, 4779. See the cited literatures.

(17) Werkman, P. J.; Wieringa, R. H.; Vorenkamp, E. J.; Schouten, A. J. *Langmuir* **1998**, *14*, 2119.

(18) Jaeger, D. A.; Reddy, V. B.; Arulsamy, N.; Bohle, D. S. *Langmuir* **1998**, *14*, 2589.

(19) Soyer, H.; Mingotaud, C.; Boillot, M.-L.; Delhaes, P. *Langmuir* **1998**, *14*, 5890.

(20) Haga, M.; Kato, N.; Monjushiro, H.; Wang, K.; Hossain, Md. D. *Supramol. Sci.* **1998**, *5*, 337.

(21) Lu, X.; Zhang, Z.; Liang, Y. *J. Chem. Soc., Chem. Commun.* **1994**, 2731; *Langmuir* **1996**, *12*, 5501; *Langmuir* **1997**, *13*, 533.

(22) Iida, M.; Yonezawa, A.; Tanaka, J. *Chem. Lett.* **1997**, 663.

(23) Iida, M.; Tanase, T.; Asaoka, N.; Nakanishi, A. *Chem. Lett.* **1998**, 1275.

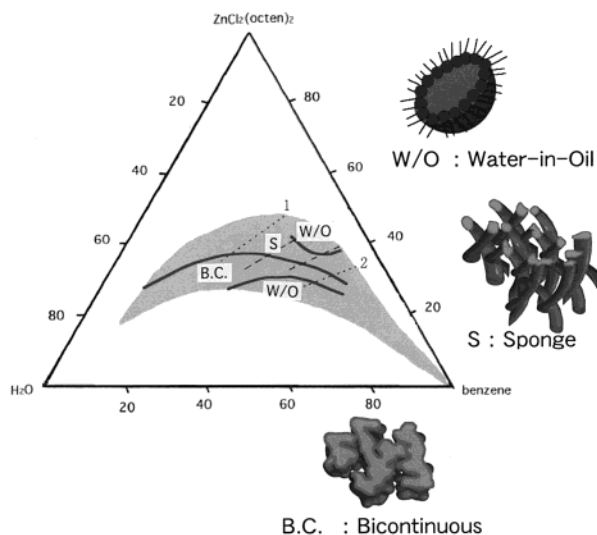


**Figure 1.** Phase diagram for ternary system of  $\text{Zn}(\text{oct-en})_2\text{Cl}_2$ /water/benzene and models of microemulsions: broken line, IR measurement; dotted line, spin-echo NMR measurement.

water. Aggregation of  $\text{Zn}(\text{oct-en})_2\text{Cl}_2$  in the mixed solvents has been established on the basis of vapor pressure osmometry, and extensive motion restriction of the zinc complex and water molecules due to aggregation in the ternary systems has been suggested on the basis of NMR relaxation measurements. The solubility of a metal complex and its ability to form self-assemblies in the ternary system depend not only on solvents but also on counterions. The crystalline structure and solubility of  $\text{Zn}(\text{oct-en})_2(\text{NO}_3)_2$  have also been examined.<sup>23</sup> The solubility behavior of the above two compounds, which have different counterions, is largely identical, and transparent solutions appear at an appropriate mixing ratio of solvents. However, no studies have characterized the transparent area in the previous reports.

The transparent area was divided into separate homogeneous regions in the present study, and the aggregation structure of each region was clarified by transmission electron microscopy (TEM), atomic force microscopy (AFM), Fourier transform infrared (FT-IR) spectroscopy, and the Fourier transform pulsed-gradient spin-echo (FT-PGSE) NMR method. The molecular arrangements of the aggregation structures were examined. To the best of our knowledge, this is the first study to observe an aggregation structure in the ternary system of metal complex/oil/water.

### Experimental Section

$\text{Zn}(\text{oct-en})_2\text{Cl}_2$  was synthesized by mixing  $\text{ZnCl}_2$  with oct-en (molar ratio 1:3) in ethanol:water (volume ratio 3:2) mixed solvent under stirring.<sup>22</sup> After evaporation of the solvent, the crude  $\text{Zn}(\text{oct-en})_2\text{Cl}_2$  was extracted into chloroform from a water/chloroform system and recrystallized from ethanol. The purity of the crystal was determined by elemental analysis (Anal. Found: C, 49.90%; H, 10.03%; N, 11.56%. Calcd: C, 49.95%; H, 10.06%; N, 11.65%) and  $^{13}\text{C}$  NMR spectra. Benzene was obtained commercially and dried by molecular sieves (3A 1/16). Water was purified by MILLI-Q Labo (Millipore).

$\text{Zn}(\text{oct-en})_2\text{Cl}_2$  was dissolved in benzene at an appropriate mixing ratio, and water was added. The mixture was incubated in a water bath at 30 °C. The transparent region, which was visually determined, is shown as a dark part in Figure 1. Solutions in the transparent region were used for microscopic observation.

TEM observation was carried out on a Hitachi H-800 electron microscope at an accelerating voltage of 100 kV. Freeze-fracture

replicas were prepared using a Balzers cryofract (BAF-400). Details of the procedure have been described elsewhere.<sup>24</sup>

AFM images were taken on a Digital Instrument NanoScope III using the contact mode for narrow areas and the tapping mode for wide areas. A droplet of the solution was dropped on freshly cleaved mica and spin-coated for 600 s at 6000 rpm. The procedure of AFM is described in detail elsewhere.<sup>16</sup>

Infrared absorption spectra were recorded on a Bio-Rad FTS 575C FT-IR spectrometer equipped with a liquid-nitrogen-cooled mercury-cadmium-telluride (MCT) detector. A prism type attenuated total reflectance (ATR) system was used, and a solution cell was set on the silica prism.  $\text{Zn}(\text{oct-en})_2\text{Cl}_2$  and benzene were mixed at a weight ratio of 1:1 or 0.7:1 in the IR cell, and water was added in a stepwise manner. At each step, the mixture was mixed under sonication and IR ATR was measured. The measurement was scanned 1024 times at 4  $\text{cm}^{-1}$  resolution.

Self-diffusion coefficients were measured by the NMR FT-PGSE technique. The measurements were performed on a JEOL FX-90 spectrometer, operating at 90 MHz for protons. The spectrometer was equipped with an apparatus producing a field gradient within the range of 0.3–1.0 T/m. Temperature was controlled within  $27 \pm 0.5$  °C with a JEOL GVT2 temperature control unit. The attenuation of the spin-echo amplitude after Fourier transformation was sampled as a function of the duration,  $\delta$ , of the applied gradient pulse ( $0.2 \text{ ms} < \delta < 7.5 \text{ ms}$ ). The  $^1\text{H}$  NMR signals were followed for  $\text{H}_2\text{O}$  and  $\text{C}_6\text{H}_6$  solvents as well as for methylene protons of the zinc(II) complex,  $\text{Zn}(\text{oct-en})_2\text{Cl}_2$ . To obtain clearer  $\text{H}_2\text{O}$   $^1\text{H}$  spin-echo signals,  $\text{C}_6\text{D}_6$  solvent was used, except for the measurements of diffusion coefficients of the  $\text{C}_6\text{H}_6$  solvent. The difference in chemical shifts between  $\text{H}_2\text{O}$  and methylene proton of the  $\text{Zn}(\text{oct-en})_2\text{Cl}_2$  was 3.1 ppm. Within the concentration range wherein the  $\text{H}_2\text{O}:\text{Zn}(\text{oct-en})_2\text{Cl}_2$  molar ratio is either too large or too small, the smaller signal is overlapped by the larger peak and the intensity of the probe peak was estimated by subtracting the tail intensity of the larger peak. The accuracy of the measured diffusion coefficients was estimated to be at most  $\pm 15\%$ .

### Results

**TEM Photographs.** TEM photographs were taken for freeze-fracture replica films prepared from 1:1 (weight ratio) solutions of  $\text{Zn}(\text{oct-en})_2\text{Cl}_2$ :benzene with various water contents. At 10 wt % water content, spherical particles with a diameter between 25 and 30 nm were uniformly dispersed. These particles must be water-in-oil (W/O) microemulsions with the water captured in the core, as estimated by their size which was more than twice the molecular length of  $\text{Zn}(\text{oct-en})_2\text{Cl}_2$  and also due to the lower water content than that of benzene. Dispersed W/O microemulsions were observed even at 14 wt % (see Figure 2), but their size was increased to 30–40 nm, depending on the degree of enlargement of the water pool in the microemulsion core.

The TEM texture changed at 20 wt % water content, as seen in Figure 3. Circular textures with widely varying diameters 30–200 nm were observed to coexist with those with a slightly elongated texture. This indicates that, with increasing water content, the structure of a microemulsion changes to the sponge structure wherein infinite water channel networks of interconnected cylinders exist in the continuous oil domain. For a solution with 40 wt % water content, TEM photograph displayed a texture of the typical bicontinuous structure, where benzene and water separate as two continuous domains. A solution with 30 wt % water content was determined to be a mixture of the sponge and bicontinuous structures, given that both textures were identified in the TEM photograph. The bicontinuous structure was observed even in a 1.5:1 solution of  $\text{Zn}(\text{oct-en})_2\text{Cl}_2$ :benzene with 50 wt % water content (see Figure 4).

(24) Imae, T.; Takahashi, Y.; Muramatsu, H. *J. Am. Chem. Soc.* **1992**, *114*, 3414.

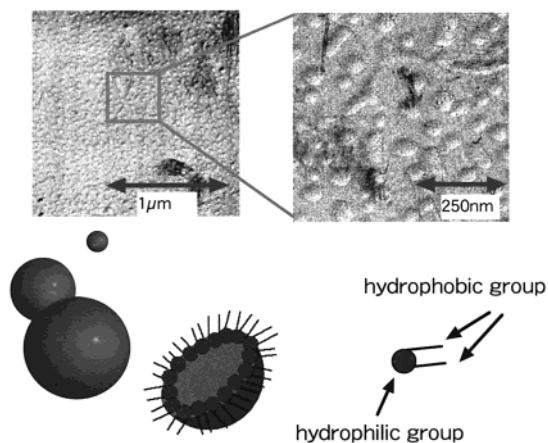


**Figure 2.** Freeze-fracture TEM photographs from a 1:1 solution of  $\text{Zn}(\text{oct-en})_2\text{Cl}_2$ :benzene with 14 wt % water content and a model of W/O microemulsion structure.

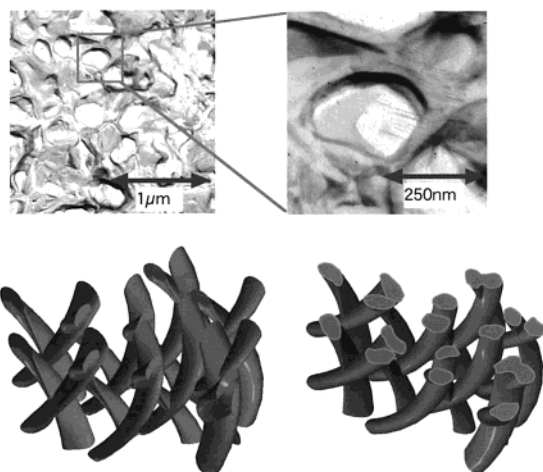


**Figure 3.** Freeze-fracture TEM photographs from a 1:1 solution of  $\text{Zn}(\text{oct-en})_2\text{Cl}_2$ :benzene with 20 wt % water content and a model of sponge structure.

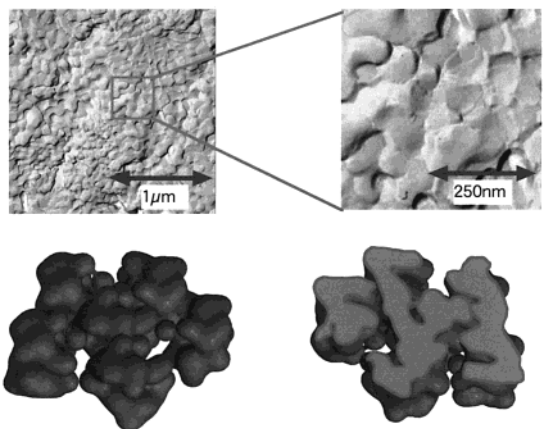


**Figure 4.** Freeze-fracture TEM photographs from a 1.5:1 solution of  $\text{Zn}(\text{oct-en})_2\text{Cl}_2$ :benzene with 50 wt % water content and a model of bicontinuous structure.

For a 0.7:1 mixing ratio of  $\text{Zn}(\text{oct-en})_2\text{Cl}_2$ :benzene, whereas the bicontinuous structure was formed in a solution with 29 wt % water content, spherical particles were found in a solution with 36 wt % water content, as shown in Figure 5. Domain regions with particles between 4 and 20 nm in diameter were determined in addition to continuous regions with particles between 20 and 40 nm

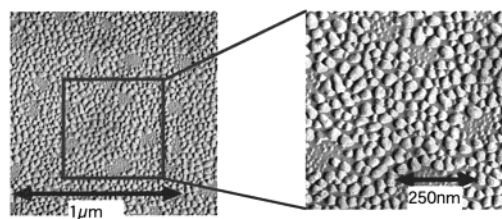


**Figure 5.** Freeze-fracture TEM photographs from a 0.7:1 solution of  $\text{Zn}(\text{oct-en})_2\text{Cl}_2$ :benzene with 36 wt % water content.

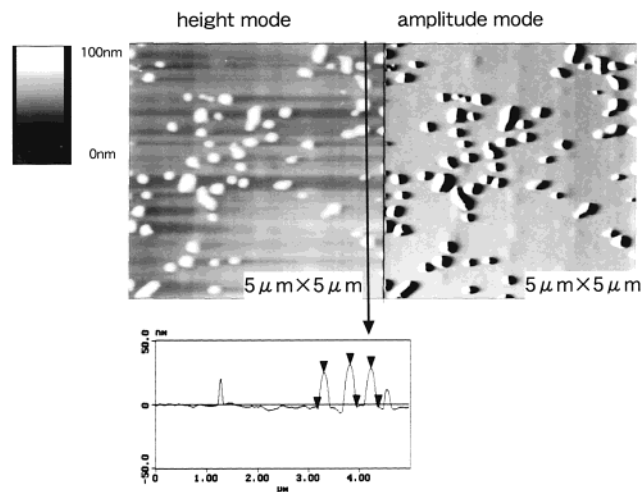


**Figure 6.** AFM images from a 1:1 solution of  $\text{Zn}(\text{oct-en})_2\text{Cl}_2$ :benzene with 14 wt % water content: left, height mode; right, amplitude mode; bottom, cross-sectional analysis lined in an image of height mode.

in diameter. Since the water content in this phase is less than that of benzene, spherical particles must be W/O microemulsions, as in the 1:1 (weight ratio) solutions of  $\text{Zn}(\text{oct-en})_2\text{Cl}_2$ :benzene with 10 and 14 wt % water contents. The more compelling evidence for the assignment of spherical particles to W/O microemulsions was obtained from the NMR FT-PGSE results, as discussed below. At a lower metal complex content ( $\text{Zn}(\text{oct-en})_2\text{Cl}_2$ :benzene = 0.5:1), both solutions with 7.7 and 11 wt % water content displayed a coexistence of sponge and bicontinuous structures.

**AFM Images.** AFM was observed in a spin-coated film prepared from a 1:1 solution of  $\text{Zn}(\text{oct-en})_2\text{Cl}_2$ :benzene with 14 wt % water content, and the image is shown in Figure 6. The size (150–200 nm diameter) of particles observed was larger than that of W/O microemulsions in the TEM photograph. Given that the height of particles was approximately 30 nm, which was consistent with microemulsion size determined by TEM, the larger diameter of the particles in the AFM texture may imply aggregation of microemulsions during preparation of the spin-coated film.

AFM images from solutions with 20, 30, and 40 wt % water contents displayed a similar texture, as illustrated in Figure 7. Given that, on the basis of TEM observations, both the sponge and bicontinuous structures are formed in these solutions, the texture must represent the interface between the two domains of benzene and water. The small area of interface in the bicontinuous structure was magnified, as shown in Figure 7. In the texture observed, spots were arranged with repeating distance of 6 Å and a tilt angle of 100°.

**IR Spectra.** The FT-IR spectra measured for 1:1 solutions of  $\text{Zn}(\text{oct-en})_2\text{Cl}_2$ :benzene with various water contents are shown in Figure 8. Band positions and their

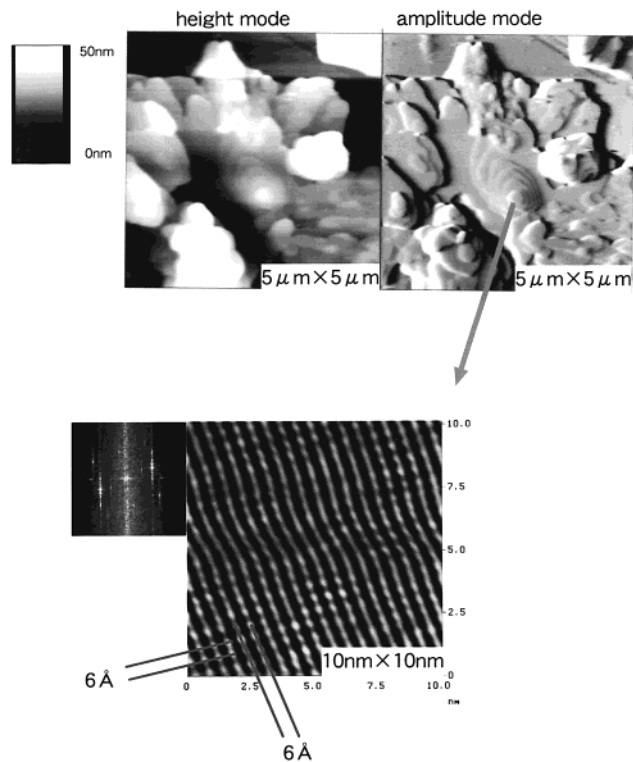


**Figure 7.** AFM images from a 1:1 solution of  $\text{Zn(oct-en)}_2\text{Cl}_2$ :benzene with 40 wt % water content: left, height mode; right, amplitude mode; bottom, magnified image (10 nm  $\times$  10 nm) at a point of interface.

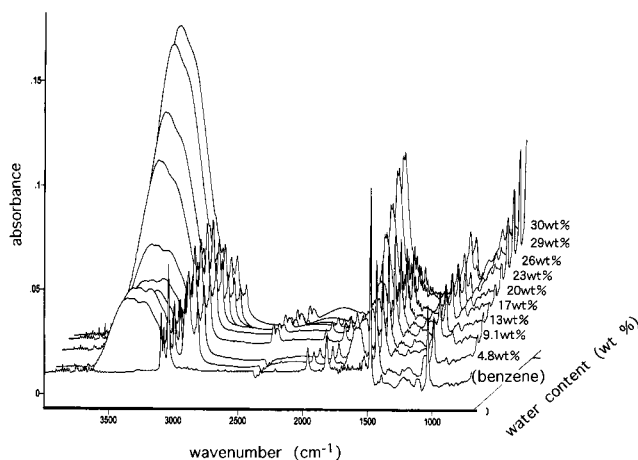


**Figure 8.** ATR IR spectra for 1:1 solutions of  $\text{Zn(oct-en)}_2\text{Cl}_2$ :benzene with various water contents. An IR spectrum of benzene is included.

assignments are listed in Table 1. Bands at 2956 and 2875  $\text{cm}^{-1}$  were assigned to  $\text{CH}_3$  asymmetric and symmetric stretching vibration modes, respectively, for alkyl chains of  $\text{Zn(oct-en)}_2\text{Cl}_2$ , and bands at 2929 and 2856  $\text{cm}^{-1}$  are due to  $\text{CH}_2$  antisymmetric and symmetric stretching vibration modes, respectively. Given that the frequencies of these bands were rather high, alkyl chains must be in a gauche conformation and not in a trans-zigzag conformation.<sup>25–28</sup> Bands at 1601, 1478, and 1094  $\text{cm}^{-1}$  are

(25) Sapper, H.; Cameron, D. G.; Mantsch, H. H. *Can. J. Chem.* **1981**, *59*, 2543.

(26) Kamata, T.; Umemura, J.; Takenaka, T.; Koizumi, N. *J. Phys. Chem.* **1991**, *95*, 4096.

(27) Tian, Y. *J. Phys. Chem.* **1991**, *95*, 9995.

(28) Myrzakozha, D. A.; Hasegawa, T.; Nishijo, J.; Imae, T.; Ozaki, Y. *Langmuir* **1999**, *15*, 6890.

**Table 1.** Band Positions and Their Assignments of ATR IR Absorption Spectra for the Ternary System of  $\text{Zn(oct-en)}_2\text{Cl}_2$ /Benzene/Water

band position <sup>a</sup> ( $\text{cm}^{-1}$ )	molecule		
	water	benzene	$\text{Zn(oct-en)}_2\text{Cl}_2$
3369 vs	hydrogen-bonded OH str		
3261 vs	hydrogen-bonded OH str		
3091 m		CH str	
3072 w		CH str	
3037 s		CH str	
2956 m			$\text{CH}_3$ asym str
2929 s			$\text{CH}_2$ antisym str
2875 sh			$\text{CH}_3$ sym str
2856 s			$\text{CH}_2$ sym str
1652 vs	OH bend		
1636 vs	OH bend		
1601 w			$\text{NH}_2$ bend (scissor)
1478 s		CH bend	$\text{CH}_2$ bend (scissor)
1094 w			$\text{NH}_2$ bend (rock)
1085 m	OH bend		
1034 m		CH bend	

<sup>a</sup> Key: vs, very strong; s, strong; m, medium; w, weak; sh, shoulder.

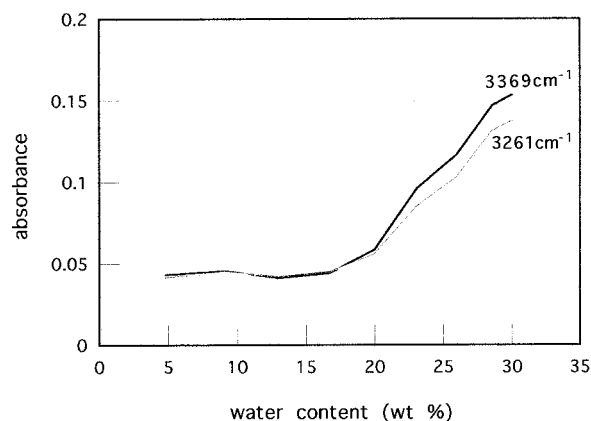


**Figure 9.** Absorbance of 3369 and 3261  $\text{cm}^{-1}$  bands as a function of water content for the ternary system of  $\text{Zn(oct-en)}_2\text{Cl}_2$ :benzene (1:1) with various water contents.

assigned to  $\text{NH}_2$  and  $\text{CH}_2$  bending modes. Bands corresponding to the CH stretching vibration modes of benzene were found at 3091, 3072, and 3037  $\text{cm}^{-1}$ . A 1478  $\text{cm}^{-1}$  band for the CH deformation mode of benzene overlapped the  $\text{CH}_2$  bending mode of alkyl chains. The other CH bending mode of benzene was observed at 1034  $\text{cm}^{-1}$ . Strong bands for hydrogen-bonded OH stretching modes of water were located at 3369 and 3261  $\text{cm}^{-1}$ , and bands of OH bending modes were at 1652, 1636, and 1085  $\text{cm}^{-1}$ .

Bands assigned to  $\text{Zn(oct-en)}_2\text{Cl}_2$  and benzene were invariable in intensity and frequency, even when water was added, due to the fact that the content ratio of  $\text{Zn(oct-en)}_2\text{Cl}_2$  and benzene were kept constant. On the other hand, vibration modes of water were intensified by adding water as estimated. However, the band intensities were not linearly varied against the water content but remarkably increased above 17 wt % water content, as seen in Figure 9. The concentration corresponds to the transition point between the W/O microemulsion and sponge structures. Similar IR spectrum behavior was also observed for 0.7:1 solutions of  $\text{Zn(oct-en)}_2\text{Cl}_2$ :benzene, and the intensity of the OH band also showed a steep increase at a similar water content.

**Self-Diffusion Coefficients.** To obtain further information on the structure of microemulsions, the NMR FT-PGSE method was also used. The self-diffusion coefficients

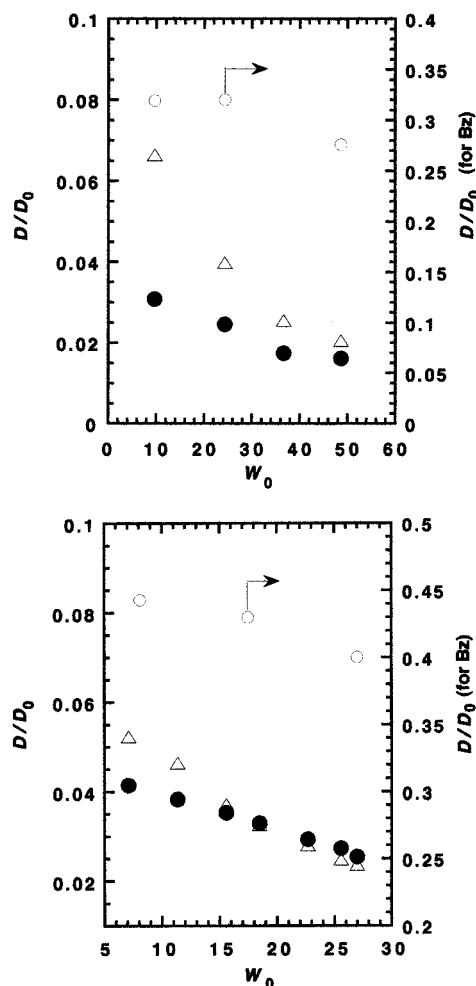


**Figure 10.** Self-diffusion coefficient ratios for water ( $\Delta$ ), benzene ( $\circ$ ), and  $\text{Zn}(\text{oct-en})_2\text{Cl}_2$  ( $\bullet$ ) depending on the water content: (top) line 1 in Figure 1 ( $\text{Zn}(\text{oct-en})_2\text{Cl}_2$  concentration in benzene is 2.26 M); (bottom) line 2 in Figure 1 ( $\text{Zn}(\text{oct-en})_2\text{Cl}_2$  concentration in benzene is 1.04 M).

( $D$ ) for water, benzene, and  $\text{Zn}(\text{oct-en})_2\text{Cl}_2$  were determined in the transparent solution region. Thus, the  $D/D_0$  ratio, where  $D_0$  corresponds to the neat solvent or the  $\text{Zn}(\text{oct-en})_2\text{Cl}_2$  monomer, was plotted against the water content ( $W_0 = [\text{water}]/[\text{Zn}(\text{oct-en})_2\text{Cl}_2]$  molar ratio) as shown in Figure 10. As  $\text{Zn}(\text{oct-en})_2\text{Cl}_2$  was hardly dissolved in neat benzene, we first determined the diffusion coefficient for  $\text{Zn}(\text{oct-en})_2\text{Cl}_2$  monomer in methanol by an extrapolation of the concentration-depending coefficients in dilute ( $0.05\text{--}0.6 \text{ mol kg}^{-1}$ ) methanol solutions where the  $\text{Zn}(\text{oct-en})_2\text{Cl}_2$  is scarcely aggregated. The value in benzene was estimated from that in methanol using the viscosity ratio,  $\eta(\text{methanol})/\eta(\text{benzene}) = 5.1/5.6$ , on the basis of the Stokes–Einstein equation. Thus, the  $D_0$  values we used were  $2.24 \times 10^{-9}$ ,  $2.26 \times 10^{-9}$ , and  $7.42 \times 10^{-10} \text{ m}^2 \text{ s}^{-1}$  for neat water, neat benzene, and  $\text{Zn}(\text{oct-en})_2\text{Cl}_2$  monomer in benzene, respectively. The following characteristic trend can be seen in the figures: The diffusion coefficient ratios are decreased significantly for all components of benzene, water, and  $\text{Zn}(\text{oct-en})_2\text{Cl}_2$  with an increase in the water content.

### Discussion

The ternary system of surfactant/oil/water is known to form different types of microemulsions. Figure 1 includes the phase diagram obtained from microscopic examination

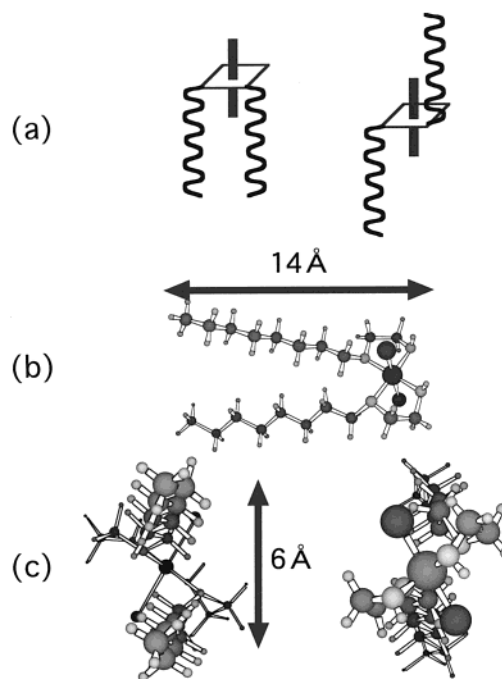


**Figure 11.** (a) *Cisoid* (left) and *transoid* (right) diastereomer, (b) side view, and (c) normal views from alkyl chain side (left) and from metal complex side (right) of *cisoid*  $\text{Zn}(\text{oct-en})_2\text{Cl}_2$ .

of the  $\text{Zn}(\text{oct-en})_2\text{Cl}_2/\text{benzene}/\text{water}$  system. In this system, a transparent area appears, which spreads from a benzene-rich region to benzene-poor region. This area is composed of four distinct regions. Each is assigned to either a W/O microemulsion, sponge, or bicontinuous structure. The regions depend on the water or  $\text{ZnCl}_2(\text{oct-en})_2$  content. In other words, the formation of microemulsions is determined by the content ratio of  $\text{Zn}(\text{oct-en})_2\text{Cl}_2$  and water in the present ternary system. It should also be noted that the equivalent weight fraction of three components locates in the bicontinuous structure, indicating equivalent domain size of benzene and water. The formation of a microemulsion in the ternary system of  $\text{Zn}(\text{oct-en})_2\text{Cl}_2/\text{benzene}/\text{water}$  is comparable with the assembly formation of *N*-alkylethylenediamine, which forms vesicles in dilute aqueous  $\text{Cu}(\text{NO}_3)_2$  or acidic solution.<sup>21</sup>

In the W/O microemulsion,  $\text{Zn}(\text{oct-en})_2\text{Cl}_2$  molecules are arranged with the headgroups directed inside the microemulsion and with the alkyl chains dispersed in continuous bulk benzene, as seen in Figures 1 and 2. With increasing water content, the microemulsions increase in size due to an expansion of the water pool. With an increase in water content over the W/O microemulsion, the IR absorption band intensity of the OH stretching vibration mode of water remarkably increases, whereas the vibration bands of  $\text{Zn}(\text{oct-en})_2\text{Cl}_2$  and benzene scarcely change. The starting point of the increase in intensity is consistent with a transition from the W/O microemulsion to the sponge structure (see Figure 9). This may indicate an increase in the amount of water within the domain of the sponge and bicontinuous structures rather than an increase within the encapsulated domain of the microemulsion. Although water and benzene domains are continuous with one another in both the sponge and bicontinuous structures (see Figures 1, 3, and 4), the water domain in the sponge structure is tubular. The cross-sectional diameters of tubes are not uniform, but scattered.  $\text{Zn}(\text{oct-en})_2\text{Cl}_2$  molecules are located within the interface between the water and benzene domains in the sponge and bicontinuous structures.

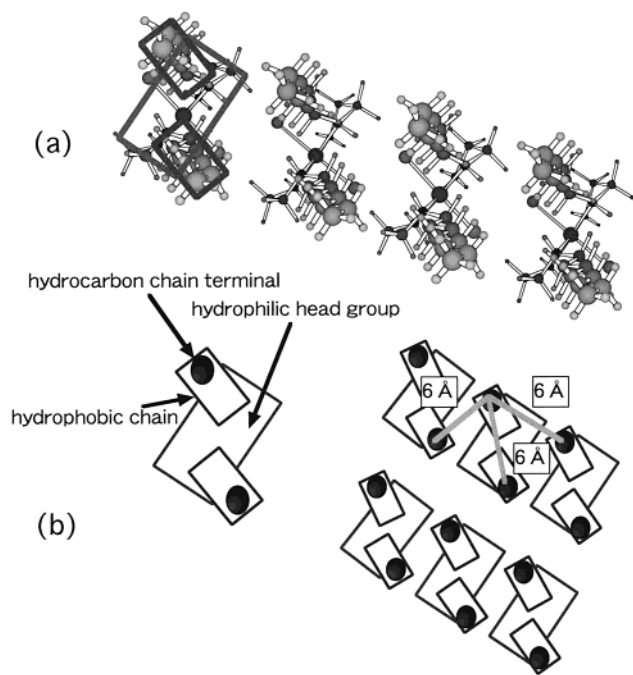


**Figure 12.** (a) Molecular arrangement of *cisoid*  $\text{Zn}(\text{oct-en})_2\text{Cl}_2$  at the interface of benzene and water domains in the bicontinuous mesophase of the ternary system of  $\text{Zn}(\text{oct-en})_2\text{Cl}_2$ : benzene (1:1) with 40 wt % water content. (b) Schematic presentation of positions of hydrocarbon terminals, hydrophobic chains, and hydrophilic headgroups in molecular arrangement (a).

Arrangement of  $\text{Zn}(\text{oct-en})_2\text{Cl}_2$  molecules at the interface between the water and benzene domains in bicontinuous structure can be assumed from the AFM image (Figure 7, bottom). The diastereomer structure of  $\text{Zn}(\text{oct-en})_2\text{Cl}_2$  is either *cisoid* (Figure 11a, left) or *transoid* (Figure 11a, right). Although the two species may coexist, the former species is selectively located at the interface between benzene and water, due to the fact that the amphiphilic structure of the hydrophilic head and hydrophobic tail is preferable. The molecular length of *cisoid* species is 14 Å and the maximum width is 6 Å, as shown in Figure 11b and c, respectively. Thus, *cisoid*  $\text{Zn}(\text{oct-en})_2\text{Cl}_2$  molecules can be arranged with a repeating distance of 6 Å between the alkyl chains in the molecule and between neighboring molecules.

Figure 12 shows (a) the most likely molecular arrangement and (b) schematic presentation of the locations of hydrophilic headgroups, hydrophobic chains, and hydrocarbon chain terminals. The arranged spots, which maintain a 6 Å separation according to the AFM image of Figure 7, are considered to be hydrocarbon chain terminals. Thus, the molecular area/single chain is approximately 36 Å<sup>2</sup>. This area is larger than the most highly packed molecular area of arachidic acid (~19 Å<sup>2</sup>),<sup>16</sup> but it is consistent with or smaller than the occupied areas of all amphiphilic metal complexes previously reported, aside from metallosoaps.<sup>15,17–20</sup> This is due to the fact that

the occupied area of the headgroup of amphiphilic metal complexes is larger than that of the hydrocarbon chain, although this depends somewhat on the metal complex species. It has been reported for bis(*N*-hexadecylethylenediamine)cobalt(III) perchlorate<sup>18</sup> that the occupied area of the *cisoid* diastereomer is different from that of *transoid*. It should be noted that the occupied area of  $\text{Zn}(\text{oct-en})_2\text{Cl}_2$  is roughly equivalent to that of the *cisoid* diastereomer. This confirms the formation of a monolayer interface by the *cisoid* diastereomer in a microemulsion composed of  $\text{Zn}(\text{oct-en})_2\text{Cl}_2$ .

With increasing water content, the self-diffusion coefficients for water, benzene, and  $\text{Zn}(\text{oct-en})_2\text{Cl}_2$  decrease continually throughout the transition between the sponge and bicontinuous structures at 36 wt % water content (line 1 of Figure 1) and throughout the transitions among sponge–bicontinuous–W/O microemulsion structures at 12 and 20 wt % water contents (line 2). The decreases in diffusion coefficients of benzene and  $\text{Zn}(\text{oct-en})_2\text{Cl}_2$  parallel to the increase in water content, as shown in lines 1 and 2, may be due to a decrease in the content of free benzene and  $\text{Zn}(\text{oct-en})_2\text{Cl}_2$ . However, this is not the case for water, for which the water content is increased. This feature is consistent with the microscopic observation that the water domain becomes smaller in the following order with an increase in the water content: sponge; bicontinuous; W/O microemulsion structures (Figures 3–5). In light of this, we monitored the root-mean-square diffusional displacements within the order of 0.1–100 μm.<sup>29</sup> Thus, it is appropriate that the phase with spherical particles in line 2 is a W/O microemulsion.

## Conclusions

Microemulsions in the ternary system of  $\text{Zn}(\text{oct-en})_2\text{Cl}_2$ /benzene/water were investigated by microscopy, spectroscopy, and spin-echo NMR. Isolated regions were shown to correspond to W/O microemulsion, sponge, and bicontinuous structures, which are commonly found in typical surfactant/oil/water systems. This indicates that the zinc(II) complex,  $\text{Zn}(\text{oct-en})_2\text{Cl}_2$ , behaves as an amphiphile once it is dissolved in mixed solvents, although it is insoluble in neat water and poorly soluble in neat benzene. The large molecular area of  $\text{Zn}(\text{oct-en})_2\text{Cl}_2$  within the interface between the benzene and water domains in the bicontinuous structure is determined by the size of the large hydrophilic metal complex. However, this area is close to that of the *cisoid* diastereomer, indicating a preferential arrangement of *cisoid* species at the interface. The diffusion coefficient of component molecules depends strongly on the structure of microemulsions. Microemulsions in solutions of amphiphilic metal complexes should prove useful for microreactions, where metal complexes as catalysts are concentrated in local areas. In particular, W/O microemulsions will predominate the catalytic reaction in encapsulated water pools.

LA000140M

(29) Stilbs, P. *Prog. Nucl. Magn. Reson. Spectrosc.* **1986**, *19*, 1.